Corresponding Author: Dr. Angela Lea Goodman, PHD

Corresponding Author's Institution: U.S. Department of Energy

First Author: Angela Lea Goodman, PHD

Order of Authors: Angela Lea Goodman, PHD; Sean Sanguinito; Barbara
Kutchko; Sittichai Natesakhawat; Patricia Cvetic; Andrew J Allen

Abstract: Shale unconventional reservoirs are currently and expected to
remain substantial fossil fuel resources in the future. As CO2 is being
considered to enhance oil recovery and for storage purposes in
unconventional reservoirs, it is unclear how the shale matrix and
fractures will react with CO2 and water during these efforts. Here, we
examined the Utica Shale and its reactivity with CO2 and water using
scanning electron microscopy, N2 and CO2 sorption isotherms, mercury
intrusion porosimetry, and X-ray scattering methods. During CO2
exposure, the presence of water can inhibit CO2 migration into the shale
matrix, promote carbonate dissolution, and dramatically change the pore
scale variability by opening and closing pore networks over the macro- to
nano-scale range. These alterations in the shale matrix could impact flow
pathways and ultimately, oil recovery factors and carbon storage
potential.

Suggested Reviewers: Maria Mastalerz
Adjunct Research Scientist, Geosciences, Indiana University
mmastale@indiana.edu
Maria is a solid background in shale and coal geology and the pore size
techniques described in this paper

Jonas (Dr. B.) Baltrusaitis
Assistant Professor, Department of Chemical and Biomolecular Engineering,
Lehigh University
job314@lehigh.edu
Jonas has a solid background in surface analysis techniques

Daniel Soeder Geology
Director of Energy Resources Initiative, Geology and Geological
Engineering (GEOL, GEOE), South Dakota School of Mines & Technology
Daniel.Soeder@sdsmt.edu
Dan has a solid background in shale and geology

Bethany Kurz

Assistant Director for Integrated Analytical Solutions, Energy &
Environmental Research Center, Energy & Environmental Research Center
burz@undeerc.org
Bethany is an active researcher working on Bakken shale and CO2

Charlie Werth
ssociate Chair for Environmental Engineering & Professor, Environmental
and Water Resources Engineering, University of Texas at Austin
werth@utexas.edu
Charlie has a strong geochemistry background

Research Data Related to this Submission

Title: shale pores
Repository: Energy Data Exchange
https://edx.netl.doe.gov/dataset/shale-pore

U.S. DEPARTMENT OF ENERGY

NATIONAL ENERGY TECHNOLOGY LABORATORY
Albany, OR • Morgantown, WV • Pittsburgh, PA

NATIONAL ENERGY TECHNOLOGY LABORATORY

October 14, 2019

To the Editor(s) of *Fuel*:

On behalf of my co-authors, I submit the manuscript "*Shale Pore Alteration: Potential Implications for Hydrocarbon Extraction and CO$_2$ Storage*" for your consideration to be published as a research article letter in *Fuel*.

In this work, we detect dramatic changes in shale pores induced by CO$_2$ and water– opening of micro-pores and closing of nano-pores. These changes have the potential to modify flow pathways in subsurface shale systems that may affect hydrocarbon recovery and carbon storage operations. These results are novel in that CO$_2$ is not expected to alter the porosity of shale systems.

This work was previously submitted to *Geophysical Research Letters* and was declined for publication. We took note of the reviewer comments to improve the manuscript. The original correspondence with this journal and reviewer comments are included at the end of this letter.

Sincerely yours,

Angela Goodman

Manuscript title: Shale Pore Alteration: Potential Implications for Hydrocarbon Extraction and CO$_2$ Storage

Corresponding author's name: Angela Goodman

Submitter's name, address, and email address: Angela Goodman, U.S. Department of Energy, National Energy Technology Laboratory, P.O. Box 10940, Pittsburgh, PA 15236, angela.goodman@netl.doe.gov, (412) 386-5347

Conflicts of interest: None

List of graphics the author would like published in color: Figures 1, 4, and 6

10/1/2019

Dear Dr. Goodman:

Thank you for submitting the manuscript "Shale Pore Alteration: Implications for Hydrocarbon Extraction and CO2 Storage" (2019GL085210) to Geophysical Research Letters. I have now received 2 reviews of the manuscript. Based on the reviews and my own reading of the manuscript, I am declining the manuscript for publication in Geophysical Research Letters.

I am enclosing the reviews, which you may find helpful if you decide to revise the manuscript and submit to another journal. I am sorry that I cannot be more encouraging at this time.

Thank you for your interest in GRL.

Sincerely,

Harihar Rajaram
Editor in Chief
Geophysical Research Letters

****
Please see the following link for information regarding GRL's Science and Presentation Category Ratings: http://publications.agu.org/author-resource-center/author-guide/grl/

Associate Editor Evaluations:

Reviewer #1 Evaluations:
Science Category (Required): Science Category 2
Presentation Category: Presentation Category B
Key Points (Required): Yes

Reviewer #1 (Comments to Author (shown to authors):

The importance of this manuscript pertains to its application to pore space alterations that occur in high organic carbon and carbonate rich shales when contact with CO2 and CO2 rich brine. It's main contribution is the distinction observed how dry CO2 and CO2 + water systems change shale pore space differently. They observe in outcrop samples that micropores within the samples increase in presence and diameter, whereas smaller pores appear to become disconnected. They support these conclusions through the use of various analytical techniques including SEM, CO2 and N2 adsorption, mercury porosimetry, and x-ray scattering techniques.

A majority of the techniques are routinely used the characterization of porous materials, but they are useful in describing some of the changes in pore space the authors set out to achieve. Heavy reliance on a paper by Zhang et al. through the introduction tended to make some rather sweeping generalizations of shales that would be rather site specific. The experimental methods feels a little light in the supporting information with almost no description in the main text, but it is just about sufficient to understand how the measurements were performed. With the execption of the xray

scattering section, that runs a bit long and potentially too in depth.

The results presented are fairly convincing in supporting the claims made by the authors, and general qualitative trends can be assumed from the data across measurement methods. The analysis of the FE-SEM data is likely very user influenced in the segmentation of the pore space, but that seems to be continuous struggle in image processing. It seemed there were certain trends from the adsorption data that could potentially be very interesting in regards to the closure and remaining porosity of the outcrop compared to the subsurface sample that are almost highlighted in Figure 3, and not clearly discussed in the text. It seems that the 400 nm pore size that remains unchanged in the x-ray scattering data would be right in range of the microporosity that you observe to be most suceptable to change from the SEM results. Why then do you not see a change in the mean pore size diameter? This seems like either the samples weren't reacted long enough, or the internal pore space of the samples wasn't being reached.

As a final thought that gave me pause in a lot of the interpretation of your results is the effect of water on the potentially accessible nanopores of the samples? Some of these techniques would be influenced by the presence of water in nanopores caused by being submerged or drawn out from the shale matrix from the affinity to dry CO2, that I'm not quite fully certain is fully avoided in the sample prepartion. Did you consider these nanometer scale capillary and confinement effects?

Reviewer #2 Evaluations:
Science Category (Required): Science Category 3
Presentation Category: Presentation Category B
Key Points (Required): No

Reviewer #2 (Comments to Author (shown to authors):

Below are my more specific comment about the paper:
Title is not really represent the content; not much in the text about hydrocarbon extraction
Key points:
First point is very general and not a contribution coming from this study. I suggest to remove it
Abstract:
Line 33 - should be added that they are very important fuel resource nowadays. Otherwise it reads well.
Introduction is to the point and reads well
Experimental methods:
The methods description is very modest. I acknowledge that the y refer to the literature and supporting information, but for the reader it would be good to know basic parameters used in each technique, as well as sample size, shape, etc. in order to get idea how to relate data from various techniques.
Results and Discussion:
Line 113 - Shales are formed under low energy environments, which lead to the creation of natural fractures that are on the millimeter scale - I do not think that low energy environment is necessarily responsible for fractures (diagenetic conditions have much to do here), and that they are on millimeter scale in shales. Many shales are massive, with no obvious fractures, especially on a millimeter scale.
Fig. 1 confused me. How does the extent pf horizontal lines for fractures and the scale in the lower right corner relate to the picture of vertical fractures? Also the drawings on the right - where do these fracture and pore sizes come from? Why, for example, organic matter pores are given as 5-750 nm? Lot of OM pore are smaller than 5 nm, and pores larger than 100 nm are rather rare. Also

where ~3800 nm width for natural fractures come from? Clearly these fractures can have variable size.

The whole page 6 included under shale properties seems misplaced. Because it is in results section I was expecting to read about properties of the shales used, rather than the introduction to shales in general. This part belongs either to introduction or some parts of discussion. Also as I have already mentioned, there are a lot of organic matter pores smaller than 5 nm, and this whole pore discussion is based on SEM that does not do well with organic pores. Also, because pores in shales are very small and larger pores are rare, it would be useful to mention classification where micropores are less than 2 nm, mesopores 2-50, and macropores above 50 nm, classification that much precedes that of Loucks et al (2012).

Line 138 - age of the Utica Shale studied should be given

Line 142 - which systems?

143 - I suggest changing to "...on the depositional and diagenetic history and mineralogical composition"

The whole part of shale properties has a lot of general discussion, yet there is no information about the shales that the geologically-inclined reader would seek, for example maturity, TOC content, mineralogical composition, age, etc. Table with this information instead of being in supporting information would be very useful in the main body of the paper.

Line 164-167 "Examining Utica samples from "outcrop" and "production zone" locations allow this work's results to be utilized in multiple applications such as understanding the Utica as a sealing unit with the outcrop sample and as a hydrocarbon reservoir and CO2 storage unit with the production sample" I am not sure how the outcrop sample would be good example of the seal. It could be weathered and changed compared to the seam units that we have subsurface.

Line 215. Results of porosimetry (Table S3) would be very useful to see in the body of text rather than in supporting information.

Fig. 3. Caption should inform us which technique was used to generate these data
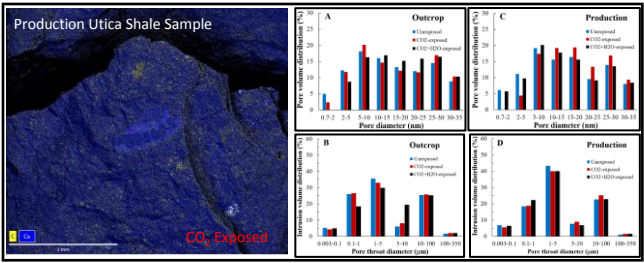Fig. 5 Mercury porosimetry does not probe pores smaller than 2 nm, this figure shows 1 nm

One of the main concerns about this paper is that when data are presented it is not clear where they come from and how they were generated. Example - line 400 mean pore diameter ~400 nm - how was this determined? Did all techniques used show similar value/

Concluding remarks are too general

O'Brian 2019 not in the reference list

Highlights (3-5):

- CO_2 is being considered to enhance oil recovery and for storage purposes in unconventional shale reservoirs
- CO_2 and water dramatically change shale pore scale variability by opening micro-pores and closing nano-pores
- These CO_2 induced alterations in shale could impact flow pathways and ultimately, oil recovery factors and carbon storage potential

Graphical Abstract (for review)

1

Shale Pore Alteration: Potential Implications for Hydrocarbon Extraction and CO$_2$

Storage

4

Angela Goodman[a], *, Sean Sanguinito[a,b], Barbara Kutchko[a], Sittichai Natesakhawat[a,c], Patricia Cvetic[a,b], Andrew J. Allen[d]

[a]United States Department of Energy, National Energy Technology Laboratory, Pittsburgh, PA 15236

[b]Leidos Research Support Team, Pittsburgh, PA 15236

[c]Department of Chemical and Petroleum Engineering, University of Pittsburgh, PA 15261

[d]Materials Measurement Science Division, National Institute of Standards and Technology, United States Department of Commerce, Gaithersburg, MD 20899

13

14

15

16

17

18

20

*corresponding author (angela.goodman@netl.doe.gov)

22

1

23 **Abstract**

24   Shale unconventional reservoirs are currently and expected to remain substantial fossil fuel

25   resources in the future. As CO_2 is being considered to enhance oil recovery and for storage

26   purposes in unconventional reservoirs, it is unclear how the shale matrix and fractures will react

27   with CO_2 and water during these efforts. Here, we examined the Utica Shale and its reactivity

28   with CO_2 and water using scanning electron microscopy, N_2 and CO_2 sorption isotherms,

29   mercury intrusion porosimetry, and X-ray scattering methods.   During CO_2 exposure, the

30   presence of water can inhibit CO_2 migration into the shale matrix, promote carbonate dissolution,

31   and dramatically change the pore scale variability by opening and closing pore networks over the

32   macro- to nano-scale range. These alterations in the shale matrix could impact flow pathways

33   and ultimately, oil recovery factors and carbon storage potential.

34

35

36

37   **Keywords (4-6):** shale, pores, CO_2, matrix, fractures, carbon storage

38

39

40

41

42

43

44

45

46

1. Introduction

With the recent shale hydrocarbon boom, shale formations in the United States are responsible for 62% of the total hydrocarbons produced [1]. In 2017, they have been shown to produce 0.382 trillion m^3 (13.5 trillion cubic feet) of natural gas and 0.78 million m^3 (4.9 million barrels) of crude oil [1]. Recovery of hydrocarbons ranges from 5 % to 30 % with high initial production rates [2]. Production rates, however, decline after the first few years by 20% of the initial rate [3]. As shales have very low permeability (<1000 nD), hydraulic fracturing is necessary to gain access to naturally-existing fractures and pore space located within the matrix to retrieve hydrocarbons and improve flow [2,4]. It has also been proposed that carbon dioxide (CO_2) can be used to enhance hydrocarbon recovery [5] and once hydrocarbons are depleted from shale, CO_2 could be stored in the reservoirs by taking advantage of newly available pore space and existing well infrastructure [6,7].

It is well known that geochemical alteration reactions in porous media are intricate processes that are difficult to measure experimentally and simulate correctly. Generally, it is believed that precipitation reactions reduce the volume of total pore space while dissolution reactions increase the volume of total pore space, however, heterogenous shale systems behave in a much more complex manner [8,9]. This complexity, due to the vast range in shale pore sizes and types, includes the potential for double layer effects that can cause ion concentration changes at nano-sized pore surfaces [10]. In addition, the interconnectivity of the shale matrix pores is variable among pore types and sizes. A recent SANS study determined that the majority of micropores are inaccessible to CO_2 and concluded that these pores would be closed for CO_2 storage purposes for Marcellus Shale [11]. They recorded no reactivity of CO_2 with the Marcellus Shale while others have observed alterations of shale with fracturing fluid [12–17], extraction cycles [18], and CO_2 [13,19–21]. Hydrocarbon extraction techniques have shown total pore volume to increase [18] while others [19] observed precipitation and dissolution reactions leading to a decrease in accessible pores with exposure to CO_2, SO_2 and O_2 with clays, feldspars, and bulk shale as caprocks.

Here, we focus on the Utica Shale play and its reactivity with CO_2 and water. Currently, 663.5 billion cubic feet of natural gas and oil are produced annually from the Utica in Eastern Ohio. The Utica Shale is a key play for hydrocarbon resources and will continue to be so far into

77 the future [22,23]. In this work, we examine how fluids interact in the natural fractures and

78 matrix pores of the Utica Shale, how these alterations affect flow pathways, and ultimately how

79 these interactions impact hydrocarbon production and CO_2 storage at the reservoir scale. Using

80 field emission - scanning electron microscopy (FE-SEM) coupled with energy dispersive X-ray

81 spectroscopy (EDS), CO_2 and N_2 sorption isotherms, mercury intrusion porosimetry, and small-

82 angle X-ray scattering methods, this effort aims to 1) quantify alterations in the shale matrix

83 from reaction with supercritical CO_2 and water, 2) link these alterations with the different pore

84 types in shale, and 3) discuss implications on whether matrix scale alterations affect transport

85 flow pathways in the shale reservoir. This enables us to define how this reactivity plays a role in

86 hydrocarbon extraction and future carbon dioxide storage operations [8–10,18,24–26].

87

88 2. Shale Properties

89   Shales are formed under low energy environments from the compaction of silt and clay-

90 size particles. This compaction process squeezes fluids out and forms natural fractures that are

91 on the millimeter aperture scale and small pores in the matrix that range from micrometers to

92 nanometers in size due lithification processes [30]. The schematic in **Figure 1** depicts a well-

93 scale view of a hydraulically fractured shale with labels for the horizontal well, hydraulic

94 fractures, natural fractures, and pores found in the matrix. The hydraulic fractures (> 10,000 nm

95 wide) are necessary to gain access to naturally-existing fractures and pore space located within

96 the matrix to retrieve hydrocarbons and improve flow [2]. Natural fractures (< 4000 nm wide)

97 are vital to hydrocarbon production as they play a key role in storage and transport of

98 hydrocarbons by connecting the matrix to the induced hydraulic fractures. It should be noted,

99 however, that natural fractures may be naturally cemented closed with calcite or bitumen [31]. In

100 any case, shale matrix pores comprise 99 % of the shale pore/void volume and are categorized as

101 inter-particle, intra-particle, and organic matter pores [31–38]. Inter-particle pores (< 2000 nm)

102 are found between the mineral grains and crystals, intra-particle pores (< 2000 nm) occur within

103 the mineral particles, and organic matter pores (< 750 nm) exist within the organic matter present

104 [31]. Shale pores are further classified by size by [31] where macropores range between 256 mm

105 and 4 mm, mesopores range between 4 mm and 62.5 μm, micropores range between 62.5 μm

106 and 1 μm, nanopores range between 1 μm and 1 nm, and picopores are less than 1 nm in size.
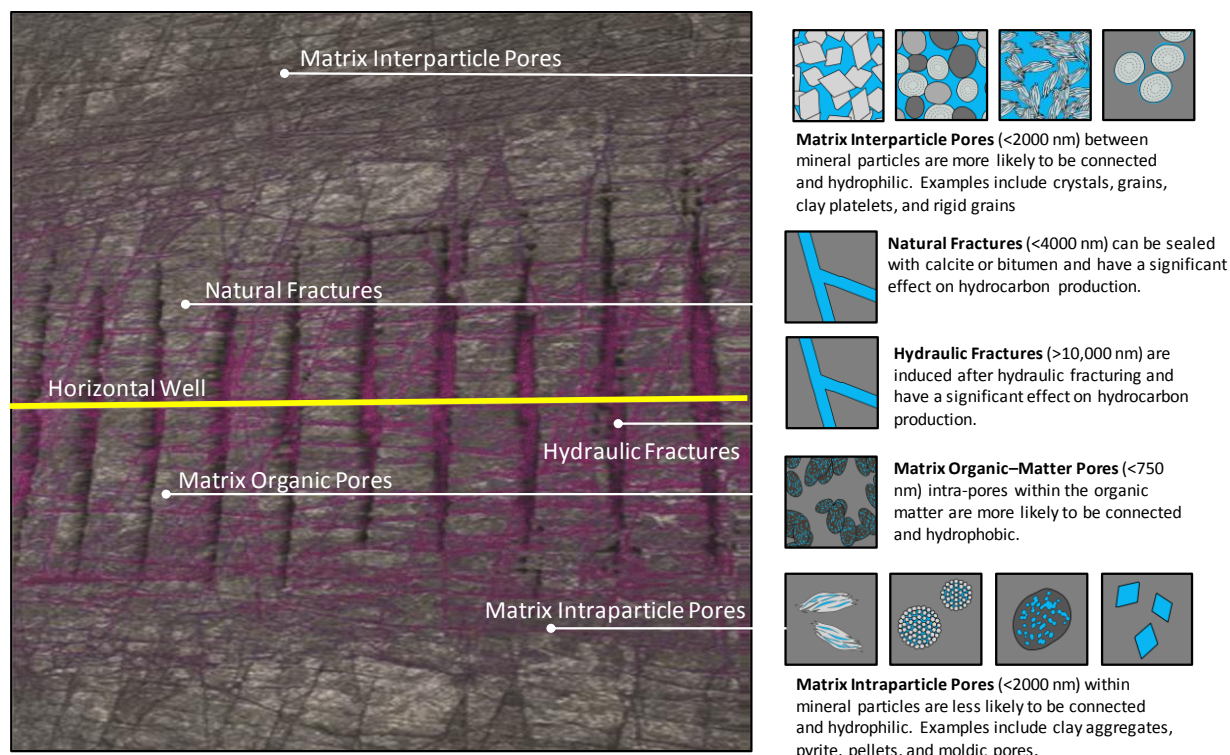
Figure 1. Well-scale view of a horizontal well in shale with hydraulic fractures, natural fractures, and matrix pores (modified from[6,31])**. Injected CO$_2$ accessing the fractures and matrix is represented in magenta.**

The Utica Shale is an Upper Ordovician mudstone with intervals of calcareous siltstone and limestone. The Utica Shale formation lies beneath portions of Ohio, West Virginia, Pennsylvania, Kentucky, Maryland, New York, Tennessee, Virginia and Canada. However, oil and gas production have been primarily focused in Eastern Ohio. It is important to note that each shale formation is complex with high variability. The pore networks for each of these shale systems are different and depend on the depositional and diagenetic history and mineralogy composition present. In some cases, it has been observed that a dominant pore type will prevail for each shale system in terms of inter-particle, intra-particle, and organic matter pores (See Figure 1) [31]. Arkakani et al. [39] characterized the porosity of Utica Shale and found inter-particle mineral pores to be the main control on total porosity as opposed to organic matter pores. They reported the importance of major pore types for Utica Shale in a decreasing order as 1) inter-particle inorganic matrix porosity, 2) organic matter porosity, and 3) fracture porosity. They

124 also noted that the natural fracture network was filled with calcite, dolomite, and bitumen. This
125 analysis is consistent with the Utica core description provided by [40] as a fine-grained shale
126 interbedded with organic-rich and fossiliferous calcareous components.

127   Utica Shale samples (Table 1) were collected from a stream bed outcrop in New York
128 state as part of the Utica Shale Flat Creek Member (referred in the text as "outcrop") and from a
129 natural gas production zone from a vertical well at depth of 3,259 m (10,692 ft) drilled in Eastern
130 Ohio as part of the Utica-Point Pleasant Member (referred in the text as "production"). Both
131 samples contain a high percentage of inorganic carbonate, however, only the production sample
132 contains high organic carbon content (Table 2). The high mineral content is consistent with the
133 finding that inter-particle mineral pores influence total porosity as opposed to organic matter
134 pores [40]. The production sample from this depth was highly fractured and was not intact as a
135 whole core [40] and contained thin clay layers, organic rich sections, and calcareous, fossil rich
136 sections.

137

138 **Table 1. Characterization of geologic samples**

Utica Sample	Description			Sample Location	
Outcrop	Stream Bed Outcrop in New York State	Appalachian Basin	Flat Creek Member	42° 53' 11" N	74° 33' 53" W
Production	Herrick 3H well core (3259 m) Monroe County, OH	Appalachian Basin	Point Pleasant Member	39° 38' 44" N	80° 57' 59" W

139

140 **Table 2. Carbon Analysis**

Utica Sample	Total Carbon		Total Inorganic Carbon		Total Organic Carbon	
	Carbon (%)	Std. Dev.*	Carbon (%)	Std. Dev.*	Carbon (%)	Std. Dev.*
Outcrop	9.86	0.08	9.41	0.14	0.45	0.17
Production	8.76	0.00	4.39	0.00	4.37	0.00

141   *Standard deviations based on two to three independent measurements of each sample

3. Experimental Methods

143   FE-SEM, volumetric isotherms, mercury intrusion porosimetry, and X-ray scattering
144 techniques were used to analyze Utica Shale outcrop and production zone samples in the
145 following three scenarios: 1) unexposed (as received samples), 2) CO_2 exposed (pressurized
146 using CO_2 to reservoir conditions), and 3) CO_2 and H_2O exposed (submerged in Milli-Q water
147 and pressurized using CO_2 to reservoir conditions). Methods for preparation of reacted samples
148 as well as detailed experimental methods are described prior work [20,21,27] and here.

3.1 Total Carbon Analysis

150   described prior work, a UIC CM014 carbon dioxide coulometer integrated with a
151 CM5130 acidification module and a CM5300 combustion furnace apparatus was used to measure
152 the total inorganic carbon (TIC), total carbon (TC), and total organic carbon (TOC) mass content
153 of the shale samples [20].

3.2 Autoclaves

155   Utica Shale samples were exposed to dry CO_2 and water in autoclave vessels. The
156 samples were placed in 500 mL polytetrafluoroethene (PTFE) lined containers which were then
157 placed in the autoclave. For the dry CO_2 exposure, the autoclave was heated to 40 °C and
158 pressurized to 10.3 MPa with dry supercritical CO_2 for a duration of 14 d. For exposure to CO_2
159 and water, the samples were submerged in 100 mL of Milli-Q ultrapure water in the 500 mL
160 PTFE lined containers. The autoclave was heated to 40 °C and pressurized to 10.3 MPa with dry
161 supercritical CO_2 for a duration of 14 d. The autoclave was then depressurized slowly over 5 h
162 to 6 h.

3.3 N_2 and CO_2 volumetric isotherms

164   A Quantachrome Autosorb 1-C surface area analyzer was used to perform volumetric
165 sorption isotherm analysis. The samples were analyzed at three different conditions: unexposed,
166 CO_2-exposed, and CO_2 + H_2O-exposed. Before the samples were analyzed, the samples were
167 degassed at 110 °C for 4 h under vacuum. While the measurements were conducted, the samples
168 were kept at a constant temperature of -196 °C and 0 °C for N_2 and CO_2, respectively. The

169   Brunauer-Emmett-Teller (BET) surface area was calculated from the adsorbed volume of N_2

170   between the relative pressure (P/P0) from 0.1 to 0.3. In addition to BET, the density functional

171   theory (DFT) method was used to determine the volume and size distribution of pores with

172   varying sizes between 0.3 nm and 35 nm. The quenched solid density functional theory

173   (QSDFT) model was used to fit the N_2 adsorption isotherms whereas, the non-local density

174   functional theory (NLDFT) model was used with the CO_2 adsorption isotherms.

175   *3.4 Mercury intrusion porosimetry*

176   A Micromeritics Autopore 9620 mercury (Hg) intrusion porosimeter was used to

177   determine the intrusion volume distribution and pore size distribution between 0.003 μm and 350

178   μm for the unexposed, CO_2-exposed, and CO_2 + H_2O-exposed samples. In addition, it was used

179   to determine the shale mass densities (bulk and skeletal).   Shale samples of mass between 0.2 g

180   and 0.3 g were first degassed under vacuum at room temperature for 2 h before being analyzed.

181   The pressure during measurements ranged from atmospheric pressure ($\approx$ 100 kPa) to

182   approximately 410 MPa.

183   *3.5 Scanning electron microscopy*

184   Scanning electron microscopy (SEM) was conducted on the Utica Shale samples without

185   a conductive coating under low vacuum using a FEI Quanta 600 FEG environmental-scanning

186   electron microscope equipped with energy dispersive X-ray spectroscopy (EDS). SEM images

187   were collected for each sample under the following three scenarios: unexposed, CO_2-exposed,

188   and CO_2 + H_2O-exposed samples. The post-exposure images were completed using a feature

189   relocation method described by our prior work [14] and [28]. To provide insight into the physical

190   morphology of these samples, secondary electron (SE) images were taken.   Backscattered

191   electron (BSE) images were taken in conjunction with EDS analysis to determine the different

192   phases within the samples. This phase differentiation is possible because EDS uses the

193   brightness within the BSE image to correlate phase composition to the average atomic number of

194   the constituting minerals.

195   *3.6 X-ray scattering methods*

196   Ultra-small-angle, small-angle and wide-angle X-ray scattering (USAXS, SAXS and

197   WAXS) measurements were carried out at the Advanced Photon Source (APS), Argonne

198   Laboratory, Argonne, IL, USA, specifically the APS USAXS facility at APS sector 9-ID using

199   an X-ray energy of 21 keV. See Appendix A for additional details.

200   SAXS measurements were made using a Pilatus 100K 2D detector (Dectris AG, Baden,

201   Switzerland) and sector-averaged to provide scattering intensity data in the range 0.5 nm^{-1} $< q <$

202   17 nm^{-1} with a q resolution of ≈ 0.06 nm^{-1}. Geometrical calibration of the SAXS detection

203   geometry is obtained using a silver behenate small-angle diffraction standard. SAXS intensities

204   are not necessarily absolute-intensity-calibrated but can be normalized to the USAXS data (using

205   data in the overlap regime). By combining USAXS and SAXS data, absolute-intensity calibrated

206     $I(q)$ *versus* q were obtained over the contiguous range of 0.001 nm^{-1} $< q < 17$ nm^{-1}.

207   WAXS measurements were made using a modified Dectris Pilatus 300KW 2D detector

208   and sector-averaged to provide X-ray diffraction (XRD) intensity *versus* q over a range 13.5 nm^{-1}

209     $< q < 62.5$ nm^{-1} with a q resolution of ≈ 0.09 nm^{-1} (slightly coarser than for SAXS due to a

210   smaller sample-to-detector distance). The WAXS instrument geometry (and q) was calibrated

211   using NIST Standard Reference Material, SRM 660a (LaB6: lanthanum hexaboride)[29].

212   Powdered samples for the unexposed, CO_2-exposed, and CO_2 + H_2O-exposed samples

213   (thickness of order 100 µm) were encapsulated in plastic tape, mounted on a sample paddle, and

214   USAXS, SAXS and WAXS measurements made in sequence. The total data collection time for

215   each sample was ≈ 6 min. The beam size was 0.8 mm horizontal by 0.8 mm vertical for

216   USAXS, and 0.8 mm horizontal by 0.2 mm vertical for SAXS and WAXS.

217

4. Results and Discussion

4.1 Chemical Reactivity of CO_2 and H_2O with Shale

220   In our recent work, we found that CO_2 alone sorbs to the clay and kerogen components

221   and reacts with the carbonate portion of dry Utica Shale by extracting interstitial water from the

222   interior clay layers to etch and pitch the shale matrix. When the shale was exposed to CO_2 and

223   H_2O, CO_2 primarily dissolves in the water layer instead of sorbing to the clay and kerogen

224   components [20,21]. H_2O in this case acts as a barrier and prevents access of CO_2 to the kerogen

225 and clays while accelerating the dissolution of carbonate regions in the Utica Shale, which in
226 turns expands etching and pitting of the shale.

227   In this work, FE-SEM illustrates the etching, pitting, and changes at the micro-pore scale
228 from carbonate dissolution and precipitation in the outcrop Utica Shale samples before and after
229 reaction with CO_2 and water (see Figure 2). FE-SEM characterization primarily show the calcite
230 matrix, quartz, and pyrite grains of the outcrop Utica sample. In Figure 2A, the images display
231 FE-SEM backscattered (BSE) images of unexposed Utica Shale (left), supercritical CO_2 exposed
232 Utica Shale (middle), and supercritical CO_2 and water exposed Utica Shale (right). These images
233 are of the same location before and after exposure to CO_2 and water. Minor etching and changes
234 in porosity occur from CO_2 exposure (middle), while major etching, pitting, and changes in
235 porosity are apparent after CO_2 and water exposure (right) during carbonate dissolution. These
236 changes in porosity were quantified using the open-source software packages Ilastik and ImageJ
237 for interactive image classification and the results are shown in Figure 2B. These bottom images
238 are the same FE-SEM BSE images shown in the top of the figure, however, these images were
239 modified, segmented, enhanced, and analyzed to quantify changes in porosity. In Figure 2B,
240 porosity is color-coded as white, while solid space is color-coded as black. The image analysis
241 shows that porosity increased to 7.6 % following CO_2 exposure and then to 33 % following CO_2
242 and water exposure for micro-pores between 1000 nm and 15,000 nm.

243

244

	Unexposed	CO₂-Exposed	CO₂ + H₂O - Exposed

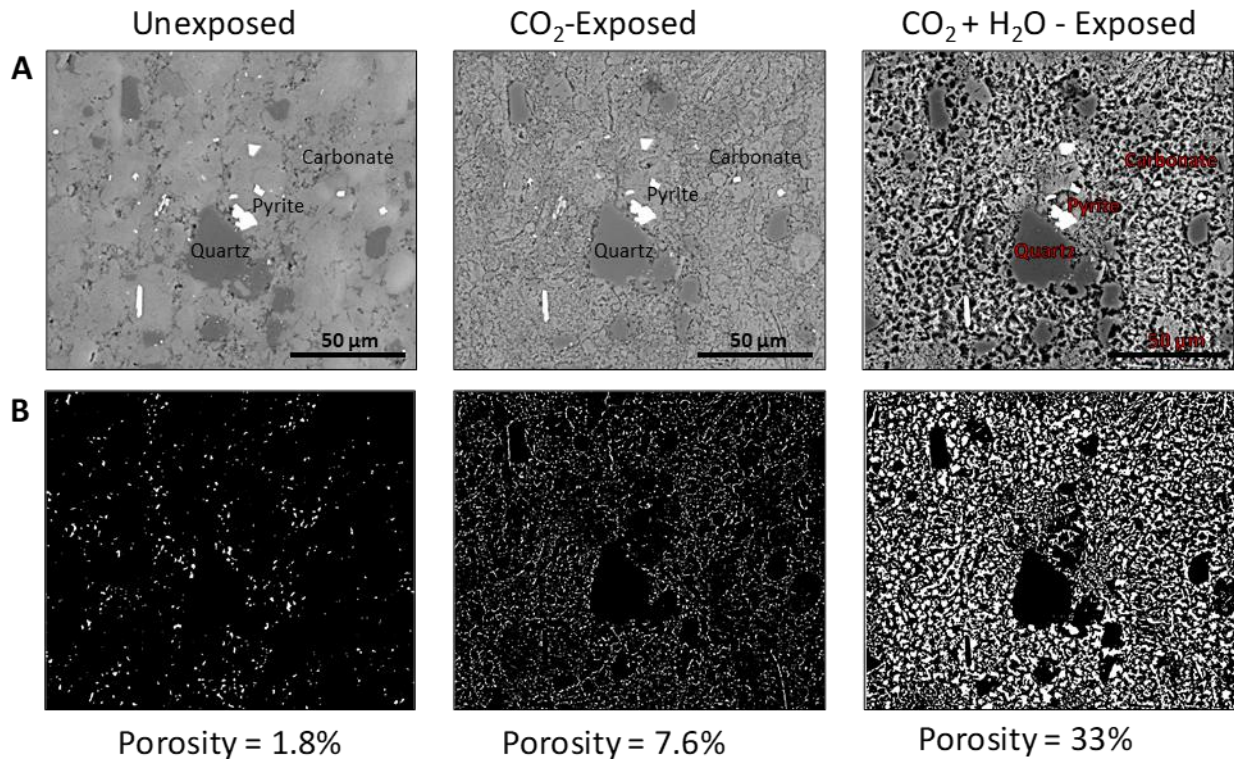Porosity = 1.8%   Porosity = 7.6%   Porosity = 33%

245

Figure 2. **A: Field-emission scanning electron microscopy backscattered (FE-SEM BSE) images of outcrop Utica Shale unexposed (left), supercritical CO_2 exposed (middle) and supercritical CO_2 and water exposed (right). B: The same FE-SEM BSE images shown in A, however, modified with Ilastik and ImageJ where porosity is color-coded as white and solid space is color-coded as black.**

For the production Utica Shale sample, high-resolution FE-SEM measurements were initiated on the unexposed sample. Unfortunately, an image set complimentary to the Utica outcrop samples (see Figure 2) was unsuccessful as the production sample did not remain intact during reaction with CO_2 due to its thin and fractured nature. Figure 3 illustrates the fractured nature of the production sample after reaction with CO_2. FE-SEM using EDS revealed higher levels of organic matter (see yellow bands in Figure 3) in the production sample when compared to the outcrop sample. Unfortunately, the reactivity of the organic content could not be explored as additional at depth production samples could not be secured.
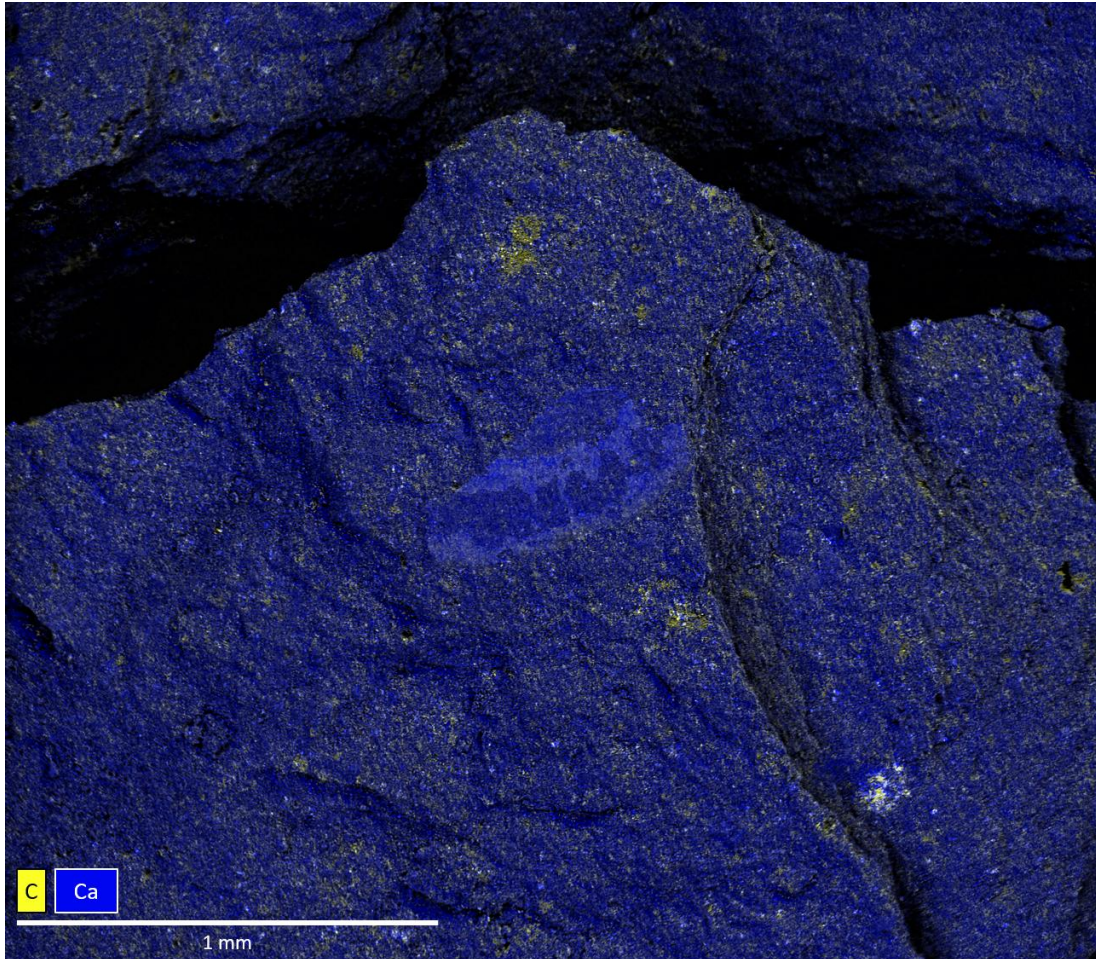
259

11

260

Figure 3. Scanning electron energy dispersive X-ray spectroscopy image of a production zone Utica Shale exposed to dry CO_2 at reservoir conditions. Blue regions are calcite rich indicating carbonate presence while yellow bands represent carbon or organic matter.

264

Alteration of pore sizes of the outcrop and production Utica Shale samples were also documented with CO_2 and N_2 sorption isotherm measurements and Hg intrusion porosimetry measurements. The combination of these two techniques allows us to examine the impact on the Utica Shale pore volumes and pore size distributions after exposure to CO_2 and H_2O from the picopores to mesopores range (i.e., 0.3 nm to 350 μm [350,000 nm]). Textural properties of the outcrop and production samples in terms of bulk density, apparent density, BET surface area, and pore volume were compiled (Table 3).

272

Table 3. Textural properties of the Utica outcrop and production samples

274

Parameter	Outcrop			Production		
	Un-exposed	CO_2-exposed	$CO_2 + H_2O$-exposed	Un-exposed	CO_2-exposed	$CO_2 + H_2O$-exposed
Bulk density $(g/cm^3)^a$	1.1620	1.1869	1.0742	1.0786	1.0970	1.0381
Apparent density $(g/cm^3)^a$	2.7114	2.5247	2.3665	2.8299	2.8815	2.5089
BET surface area $(m^2/g)^b$	6.8	6.3	5.8	19.6	8.2	17.5
Surface area $(m^2/cm^3)^c$	7.9	7.5	6.2	21.1	9.0	18.2
Diameter, d < 0.7 nm[d]	0.00127	0.00141	0.00139	0.00463	0.00371	0.00423
d = (0.7 to 2) nm[e]	0.00071	0.00030	0.00001	0.00223	0.00000	0.00181
d = (2 to 35) nm[e]	0.01177	0.01239	0.01651	0.03429	0.02433	0.03172

275   [a]Measured from Hg intrusion porosimetry. Total intrusion volume uncertainty is ± 0.03 cc/g and
276   median pore diameter uncertainty is ± 5.0 nm. [b]Measured from N_2 isotherm at -196 °C and
277   relative pressures between 0.1 and 0.3. Estimated instrumental measurement uncertainties are
278   within ± 5 %. [c]Surface area = BET surface area x bulk density. [d]Measured from CO_2 isotherm at
279   0 °C. [e]Measured from N_2 isotherm at -196 °C.

280

      Data compiled in Tables 4 and 5 show that pore sizes from N_2 isotherms of 15 nm or less
282   become less accessible, where in some cases a 100% decrease in pore volume is observed.
283   Meanwhile, pore sizes of 15 nm or more become more accessible after reaction with $CO_2 + H_2O$,
284   where in some cases a 32% increase in pore volume is calculated (see Appendix A Figures A1
285   and A2 and Tables A1 and A2 for CO_2 isotherms and Hg porosimetry data). Figure 4 highlights
286   a portion of these changes from Tables 4 and 5 in pore size distributions in the 0.7 nm to 2 nm
287   and 5 μm to 10 μm ranges for both the outcrop and production samples. While both samples
288   reveal a multi-modal distribution, the inset in Figure 4 records the alteration in pore volume

distributions of the outcrop and production. Between 0.7 nm and 2 nm, the outcrop pore volume changes from 5% to 0% after reaction with CO_2 and H_2O while the production pore volume changes from 6.1% to 5.7%. Between, 5 μm and 10 μm, the outcrop pore volume changes from 6.0% to 19.5% after reaction with $CO_2 + H_2O$ while the production pore volume changes from 7.7% to 6.9%. Carbonate dissolution and precipitation are likely responsible for opening of the larger, micro-pores and are consistent with the 30% increase in porosity estimated from FE-SEM image analysis (see Figure 2). Aggregation of clay and organic features and precipitating particles may be responsible for the decrease in the smaller, nano-pores [41]

Table 4: Percent Pore volume distribution from N_2 isotherms <u>for the outcrop Utica Shale</u>. The numbers in the parentheses are percent volume changes relative to the values of the unexposed sample. See Table 3 for uncertainties.

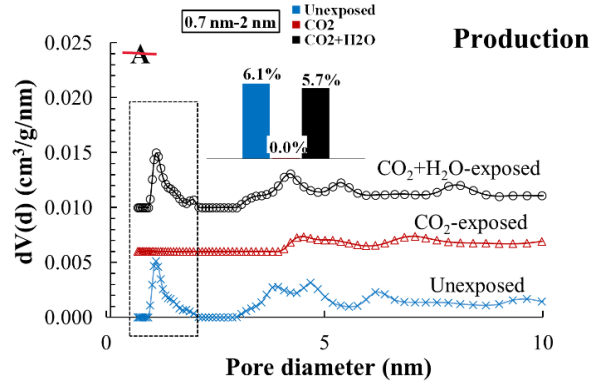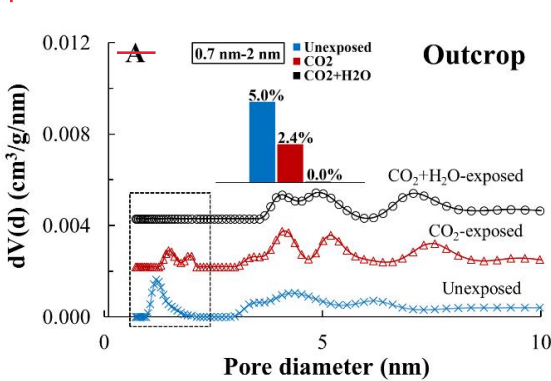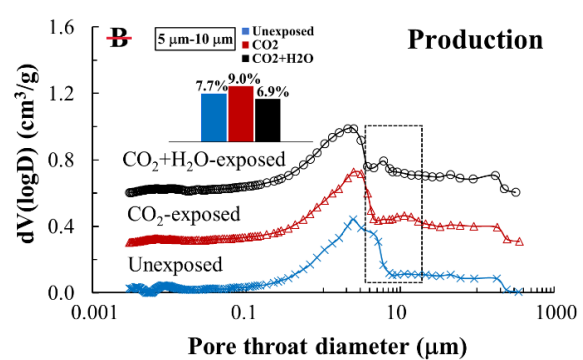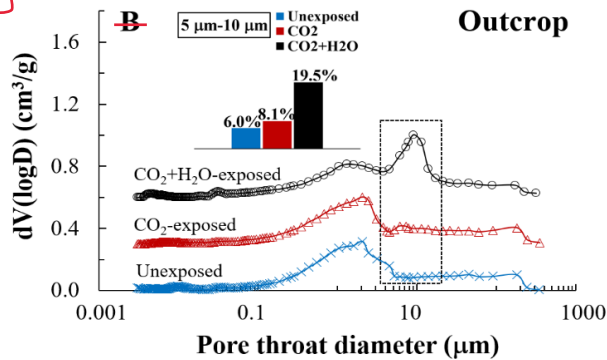| Pore diameter range (nm)	Unexposed	CO_2-exposed	$CO_2 + H_2O$-exposed
0.7 to 2	5.0	2.4 (-52.7)	0.0 (-100.0)
2 to 5	12.2	11.8 (-4.0)	8.8 (-28.5)
5 to 10	18.1	20.2 (+11.4)	16.3 (-9.8)
10 to 15	16.1	14.7 (-8.8)	16.9 (+5.2)
15 to 20	13.2	12.1 (-8.5)	15.2 (+14.7)
20 to 25	12.0	11.6 (-3.2)	15.9 (+32.3)
25 to 30	14.5	17.0 (+17.1)	16.5 (+13.7)
30 to 35	8.8	10.3	10.3

| | | (+16.8) | (+17.0) |

Table 5: Percent Pore volume distribution from N_2 isotherms <u>for the production Utica Shale</u>. The numbers in the parentheses are percent volume changes relative to the values of the unexposed sample. See Table 3 for uncertainties.

Pore diameter range (nm)	Unexposed	CO_2-exposed	$CO_2 + H_2O$-exposed
0.7 to 2	6.1	0.0 (-100.0)	5.7 (-6.3)
2 to 5	11.2	4.4 (-60.4)	9.7 (-13.0)
5 to 10	19.1	17.4 (-9.1)	20.1 (+5.2)
10 to 15	15.6	19.2 (+23.4)	17.8 (+14.1)
15 to 20	16.4	19.4 (+18.0)	15.6 (-4.9)
20 to 25	9.6	13.3 (+39.2)	9.1 (-4.8)
25 to 30	14.0	16.9 (+20.8)	13.5 (-3.1)
30 to 35	8.0	9.4 (+16.4)	8.4 (+4.4)

309

Figure 4. Pore size distributions analyses of the outcrop and production Utica Shale samples: (A) 0.7 nm to 10 nm (from N_2 sorption isotherms) (B) 0.003 μm to 350 μm (from Hg porosimetry). Insets show corresponding pore volume distributions of the unexposed, CO_2-exposed, and CO_2 + H_2O-exposed samples for the 0.7 nm to 2 nm and 5 μm to 10 μm pore diameter ranges. Uncertainties are within ± 5% and traces are offset form each other for clarity.

317

Results from ultra-small-angle X-ray scattering (USAXS), small-angle X-ray scattering (SAXS), and wide-angle X-ray scattering (WAXS) analysis were consistent with FE-SEM, N_2 and CO_2 sorption isotherm measurements, and Hg intrusion porosimetry measurements described above. The nominal porosity ~~and surface area~~ increased as CO_2 and CO_2 and H_2O were reacted with the production Utica samples (Figure 5). Comparison of the scattering curves for the powdered shale samples, together with their respective attenuations of the transmitted X-

16

324   ray beam, indicates that the 1 μm to 4 μm size pores in the scattering size distributions are the

325   voids between the powder grains and account for most of the porosity of the powdered samples.

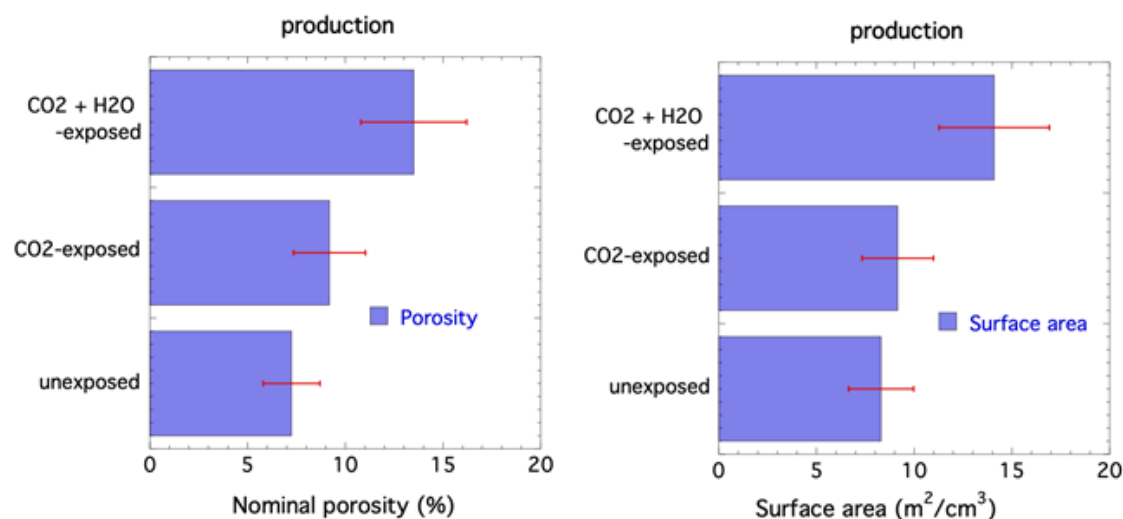326   Nano-size pores can be attributed to porosity within the solid powder grains.

327

328

329   **Figure 5: Nominal porosity ~~and surface area~~ for the production Utica Shale sample as**
330   **calculated from USAXS, SAXS, and WAXS measurements (Advanced Photon Source,**
331   **sector 9-ID). Horizontal bars in the figures represent estimated Type B standard**
332   **uncertainties (≈67% confidence) based on measurement history of similar samples** [42]**.**

333

334   **5. Implications for Hydrocarbon Extraction and CO$_2$ Storage**

335   In the schematic in Figure 6, we link the data collected in this study regarding pore

336   changes in Utica Shale following reaction with CO_2 and H_2O with the shale fracture, pore types,

337   and pore size classification system designed by Loucks et al. [31]. The green arrows represent

338   pore alteration trends identified by FE-SEM. The increase in porosity between 7 % and 33 %

339   detected with FE-SEM primarily corresponds to micro-scale changes associated with

340   intraparticle and interparticle pores in the mineral matter and natural fractures as carbonate is

341   dissolved. The blue and purple arrows represent the pore alteration trends identified by N_2 and

342   CO_2 sorption isotherm measurements and Hg intrusion porosimetry measurements, respectively.

343   The smaller pores in the nano-scale range of 2 nm to 15 nm are likely associated with clay and

344   organic features and may become inaccessible due to preferential aggregation of precipitating

345   particles in the smallest pores [41]. Orange arrows for SAXS measurements represent alteration

346   of pores in the 1 nm to 1000 nm range and further support the micro- and nano-sized changes

347   recorded with FE-SEM and pore size analysis techniques.

348

349

350

351

352

353

354

355

A. Pore-Type and Fracture Classes

Hydraulic Fractures

Natural Fractures

Interparticle Pores

Intraparticle Pores

Organic-Matter Pores

B.

CO$_2$ Sorption

N$_2$ Sorption

USAXS/SAXS/WAXS

Mercury Porosimetry

SEM

O=C=O
0.330 nm

C.

Picopore <1nm	Nanopore 1nm – 1μm (1-1000 nm)	Micropore 1μm – 62.5μm (1000-62,500 nm)	Mesopore 62.5μm – 4mm (62,500-4,000,000 nm)	Macropore 4mm – 256mm (>4,000,000 nm)

D.

356

Figure 6. Schematic linking shale fracture and pore types and size classes with the analytical techniques applied to investigate reactivity of Utica outcrop and production samples. **(A)** Fracture and pores present within mudrock: hydraulic fractures, natural fractures, interparticle and intraparticle pores associated with mineral matrix, and organic-matter pores associated with organic matrix. **(B)** Analytical techniques used to examine pore size distributions and porosity characteristics in mudrocks. **(C)** Pore-size classification developed by [31]. **(D)** Pore-size trends with Utica outcrop and production samples following reaction with CO$_2$ and H$_2$O. Green arrows represent data from scanning electron microscopy, blue arrows represent data from CO$_2$ and N$_2$ low-pressure gas sorption isotherm measurements, purple arrows represent data from mercury intrusion

19

porosimetry measurements, and orange arrows represent data from X-ray scattering

methods.

369   These results show that CO_2 and H_2O reactivity with shale can dramatically change the

370   pore scale variability by opening and closing pore networks over the meso- to nano- range. Due

371   to the heterogeneity of shales in terms of fluid content, mineralogy, TOC, thermal maturity, and

372   pore scale variability, it is important to understand the chemical reactivity of the pore network in

373   the shale matrix [43]. As described by [31], a predominant pore system likely plays a key role on

374   porosity and transport for each shale play. For the Utica, inter-particle inorganic matrix porosity

375   dominates pore distribution type followed by organic matter porosity and fracture porosity [39].

376   In quantifying flow and transport properties, the predominant pore system and the chemical

377   reactivity within this network from the macro- to nano-scale should be considered. Observations

378   specific to the Utica show that meso- and micro-pores are opening while nano-pores are closing.

379   In general, an increase in micro-porosity could translate to an increase in inter-particle pore

380   connectivity within the shale matrix with improved access to natural and hydraulic fractures.

381   This in turn, could increase CO_2 storage resource potential. On the other hand, closure of nano-

382   pores associated with organic matter porosity in the shale matrix may decrease access to

383   networks needed to improve enhanced oil recovery potential. The vast differences in alteration

384   reactions and changes in pore scale variability demonstrate the importance of linking how these

385   alterations affect flow pathways. Ultimately, flow property changes will affect hydrocarbon

386   production, CO_2 storage, and sealing units at the reservoir scale of the Utica Shale and other

387   shale plays. This is an important step in quantifying and reducing uncertainties in the porosity,

388   the degree to which the pores are connected, and how porosity can affect transport and flow

389   properties of shale systems.

390

6. Concluding Remarks

392   Porosity is a key parameter in subsurface systems such as shale formations because it is

393   directly linked to fluid storage - in this case for hydrocarbon extraction and CO_2 storage. This

394   work shows that CO_2 has the ability to alter porosity from the micro- to nano-scale. This suite of

395   complimentary techniques show that pores are both opening at the micro-scale and closing at the

396   nano-scale for Utica Shale depending on their pore type and size classification. The alteration of

397   pore scale variability may affect transport and flow properties of the shale systems and may vary

398   depending upon a shale formation's petrological properties.

399

408

424 **References**

425 [1] EIA. Annual Energy Outlook 2017 with projections to 2050. 2017.

426 [2] Zheng J, Wang Z, Gong W, Ju Y, Wang M. Characterization of nanopore morphology of
427 shale and its effects on gas permeability. J Nat Gas Sci Eng 2017.
428 doi:10.1016/j.jngse.2017.10.004.

429 [3] EIA. U . S . Energy Information Administration Year-over-year summary 2019.

430 [4] Fernø MA, Hauge LP, Uno Rognmo A, Gauteplass J, Graue A. Flow visualization of CO2
431 in tight shale formations at reservoir conditions. Geophys Res Lett 2015;42:7414–9.
432 doi:10.1002/2015GL065100.

433 [5] Wang L, Tian Y, Yu X, Wang C, Yao B, Wang S, et al. Advances in improved/enhanced
434 oil recovery technologies for tight and shale reservoirs. Fuel 2017.
435 doi:10.1016/j.fuel.2017.08.095.

436 [6] Levine JS, Fukai I, Soeder DJ, Bromhal G, Dilmore RM, Guthrie GD, et al. U.S. DOE
437 NETL methodology for estimating the prospective CO 2 storage resource of shales at the
438 national and regional scale. Int J Greenh Gas Control 2016;51:81–94.
439 doi:10.1016/j.ijggc.2016.04.028.

440 [7] Myshakin EM, Singh H, Sanguinito S, Bromhal G, Goodman AL. Numerical estimations
441 of storage efficiency for the prospective CO 2 storage resource of shales. Int J Greenh Gas
442 Control 2018;76:24–31. doi:10.1016/j.ijggc.2018.06.010.

443 [8] Emmanuel S, Anovitz LM, Day-Stirrat RJ. Effects of Coupled Chemo-Mechanical
444 Processes on the Evolution of Pore-Size Distributions in Geological Media. Rev Mineral
445 Geochemistry 2015;80:45–60. doi:10.2138/rmg.2015.03.

446 [9] Anovitz LM, Cole DR. Characterization and Analysis of Porosity and Pore Structures.
447 Rev Mineral Geochemistry 2015;80:61–164. doi:10.2138/rmg.2015.80.04.

448 [10] Stack AG. Precipitation in Pores: A Geochemical Frontier. Rev Mineral Geochemistry
449 2015. doi:10.2138/rmg.2015.80.05.

450 [11] Stefanopoulos KL, Youngs TGA, Sakurovs R, Ruppert LF, Bahadur J, Melnichenko YB.
451   Neutron Scattering Measurements of Carbon Dioxide Adsorption in Pores within the
452   Marcellus Shale: Implications for Sequestration. Environ Sci Technol 2017.
453   doi:10.1021/acs.est.6b05707.

454 [12] Lahann R, Mastalerz M, Rupp JA, Drobniak A. Influence of CO2 on New Albany Shale
455   composition and pore structure. Int J Coal Geol 2013;108:2–9.
456   doi:10.1016/j.coal.2011.05.004.

457 [13] Lu J, Nicot JP, Mickler PJ, Ribeiro LH, Darvari R. Alteration of Bakken reservoir rock
458   during CO2-based fracturing - An autoclave reaction experiment. J Unconv Oil Gas
459   Resour 2016. doi:10.1016/j.juogr.2016.03.002.

460 [14] Dieterich M, Kutchko B, Goodman A. Characterization of Marcellus Shale and
461   Huntersville Chert before and after exposure to hydraulic fracturing fluid via feature
462   relocation using field-emission scanning electron microscopy. Fuel 2016;182:227–35.
463   doi:10.1016/j.fuel.2016.05.061.

464 [15] Marcon V, Joseph C, Carter KE, Hedges SW, Lopano CL, Guthrie GD, et al.
465   Experimental insights into geochemical changes in hydraulically fractured Marcellus
466   Shale. Appl Geochemistry 2017;76:36–50. doi:10.1016/j.apgeochem.2016.11.005.

467 [16] Harrison AL, Jew AD, Dustin MK, Thomas DL, Joe-Wong CM, Bargar JR, et al. Element
468   release and reaction-induced porosity alteration during shale-hydraulic fracturing fluid
469   interactions. Appl Geochemistry 2017;82:47–62. doi:10.1016/j.apgeochem.2017.05.001.

470 [17] Jew AD, Dustin MK, Harrison AL, Joe-Wong CM, Thomas DL, Maher K, et al. Impact of
471   Organics and Carbonates on the Oxidation and Precipitation of Iron during Hydraulic
472   Fracturing of Shale. Energy and Fuels 2017;31:3643–58.
473   doi:10.1021/acs.energyfuels.6b03220.

474 [18] Zhang L, Xiong Y, Li Y, Wei M, Jiang W, Lei R, et al. DFT modeling of CO_2 and Ar
475   low-pressure adsorption for accurate nanopore structure characterization in organic-rich
476   shales. Fuel 2017. doi:10.1016/j.fuel.2017.05.046.

477 [19] Pearce JK, Dawson GKW, Blach TP, Bahadur J, Melnichenko YB, Golding SD. Impure
478   CO_2 reaction of feldspar, clay, and organic matter rich cap-rocks: Decreases in the
479   fraction of accessible mesopores measured by SANS. Int J Coal Geol 2018.
480   doi:10.1016/j.coal.2017.11.011.

481 [20] Sanguinito S, Goodman A, Tkach M, Kutchko B, Culp J, Natesakhawat S, et al.
482   Quantifying dry supercritical CO_2-induced changes of the Utica Shale. Fuel
483   2018;226. doi:10.1016/j.fuel.2018.03.156.

484 [21] Goodman A, Sanguinito S, Tkach M, Natesakhawat S, Kutchko B, Fazio J, et al.
485   Investigating the role of water on CO 2 -Utica Shale interactions for carbon storage and
486   shale gas extraction activities – Evidence for pore scale alterations. Fuel 2019;242:744–
487   55. doi:10.1016/j.fuel.2019.01.091.

488 [22] Carter, K. M., Patchen, D. G., Moore, J. P., Fakhari, M. DJGW, Solis M, Dunst BJ,
489   Anthony R V, Schmid K, Metz K, et al. A geologic study to determine the potential to
490   create an Appalachian storage hub for natural gas liquids 2017.

491 [23] O'Brien D. Utica Shale Production Reaches Record in Q4. Bus J 2019:1.

492 [24] Clarkson CR, Solano N, Bustin RM, Bustin AMM, Chalmers GRL, He L, et al. Pore
493   structure characterization of North American shale gas reservoirs using USANS/SANS,
494   gas   adsorption,   and   mercury   intrusion.   Fuel   2013;103:606–16.
495   doi:10.1016/j.fuel.2012.06.119.

496 [25] Mastalerz M, Schimmelmann A, Drobniak A, Chen Y. Porosity of Devonian and
497   Mississippian New Albany Shale across a maturation gradient: Insights from organic
498   petrology', gas adsorption, and mercury intrusion. Am Assoc Pet Geol Bull 2013.
499   doi:10.1306/04011312194.

500 [26] Zhao J, Jin Z, Hu Q, Jin Z, Barber TJ, Zhang Y, et al. Integrating SANS and fluid-
501   invasion methods to characterize pore structure of typical American shale oil reservoirs.
502   Sci Rep 2017. doi:10.1038/s41598-017-15362-0.

503 [27] Ilavsky J, Zhang F, Andrews RN, Kuzmenko I, Jemian PR, Levine LE, et al. Development

504   of combined microstructure and structure characterization facility for in situ and operando
505   studies at the advanced photon source. J Appl Crystallogr 2018.
506   doi:10.1107/S160057671800643X.

507   [28]   Kutchko BG, Goodman AL, Rosenbaum E, Natesakhawat S, Wagner K. Characterization
508   of coal before and after supercritical CO2 exposure via feature relocation using field-
509   emission scanning electron microscopy. Fuel 2013;107:777–86.
510   doi:10.1016/j.fuel.2013.02.008.

511   [29]   Black DR, Windover D, Henins A, Filliben J, Cline JP. Certification of Standard
512   Reference Material 660B. Powder Diffr 2011;26:155–8. doi:10.1154/1.3591064.

513   [30]   Yao S, Wang X, Yuan Q, Zeng F. Estimation of Shale Intrinsic Permeability with Process-
514   Based Pore Network Modeling Approach. Transp Porous Media 2018.
515   doi:10.1007/s11242-018-1091-5.

516   [31]   Loucks RG, Reed RM, Ruppel SC, Hammes U. Spectrum of pore types and networks in
517   mudrocks and a descriptive classification for matrix-related mudrock pores. Am Assoc Pet
518   Geol Bull 2012;96:1071–98. doi:10.1306/08171111061.

519   [32]   Desbois G, Urai JL, Kukla PA. Morphology of the pore space in claystones - Evidence
520   from BIB/FIB ion beam sectioning and cryo-SEM observations. EEarth 2009;4:15–22.
521   doi:10.5194/ee-4-15-2009.

522   [33]   Curtis ME, Ambrose RJ, Sondergeld CH. Structural Characterization of Gas Shales on the
523   Micro- and Nano-Scales, 2010. doi:10.2118/137693-ms.

524   [34]   Lindner EN. Review of the Effects of CO2 on Very- Fine-Grained Sedimentary Rock /
525   Shale – Part II : Clay Mineral & Shale Response to Hydration Office of Fossil Energy.
526   NETL Tech Rep Ser 2016;NETL TRS-1:68.

527   [35]   Lindner EN. Review of the Effects of CO2 on Very-Fine-Grained Sedimentary
528   Rock/Shale – Part III: Shale Response to CO2 2017. doi:10.18141/1432945.

529   [36]   Lindner EN, U.S. Review of the Effects of CO 2 on Very- Fine-Grained Sedimentary
530   Rock / Shale – Part I : Problem Definition Office of Fossil Energy 2016.

531 [37] Liu Y, Yao Y, Liu D, Zheng S, Sun G, Chang Y. Shale pore size classification: An NMR
532   fluid typing method. Mar Pet Geol 2018. doi:10.1016/j.marpetgeo.2018.05.014.

533 [38] Daigle H, Hayman NW, Kelly ED, Milliken KL, Jiang H. Fracture capture of organic
534   pores in shales. Geophys Res Lett 2017;44:2167–76. doi:10.1002/2016GL072165.

535 [39] Ardakani OH, Sanei H, Ghanizadeh A, Lavoie D, Chen Z, Clarkson CR. Do all fractions
536   of organic matter contribute equally in shale porosity? A case study from Upper
537   Ordovician Utica Shale, southern Quebec, Canada. Mar Pet Geol 2018.
538   doi:10.1016/j.marpetgeo.2017.12.009.

539 [40] Brown S, Crandall D, Moore J, Mackey P, Carr T, Panetta B. Computed Tomography
540   Scanning and Geophysical Measurements of the Utica Shale from the Herrick 3H Well
541   2018. doi:10.18141/1433313.

542 [41] Kuila U, Prasad M. Specific surface area and pore-size distribution in clays and shales.
543   Geophys Prospect 2013. doi:10.1111/1365-2478.12028.

544 [42] Taylor, Barry N, Kuyatt CE. NIST Technical Note 1297 Guidelines for Evaluating and
545   Expressing the Uncertainty of NIST Measurement Results. Technology 1994.

546 [43] Arif M, Lebedev M, Barifcani A, Iglauer S. Influence of shale-total organic content on
547   CO2   geo-storage   potential.   Geophys   Res   Lett   2017;44:8769–75.
548   doi:10.1002/2017GL073532.

549

Supplementary Material

Click here to download Supplementary Material: Pore Scale Paper (Fuel) AppendixA V2.docx

*Declaration of Interest Statement

Declaration of interests

☒ The authors declare that they have no known competing financial interests or personal relationships that could have appeared to influence the work reported in this paper.

☐The authors declare the following financial interests/personal relationships which may be considered as potential competing interests: